Journal of Magnetic Resonance 211 (2011) 143–148

Contents lists available at ScienceDirect

Journal of Magnetic Resonance

journal homepage: www.elsevier.com/locate/jmr

Low-power MRI by Frank-sequence excitation

Nadia Amor *, Bernhard Blümich

Institute for Technical and Macromolecular Chemistry, RWTH Aachen University, Worringer Weg 1, 52074 Aachen, Germany

ARTICLE INFO

Article history:
Received 2 February 2011
Revised 5 May 2011
Available online 15 May 2011

Keywords:
Low-power excitation
NMR
MRI
Polyphase perfect sequence
Frank function

ABSTRACT

Recently, a new NMR method employing an rf excitation scheme with strongly reduced power has been introduced, which is based on modulating rf pulses according to Frank sequences. For many applications, a reduction of rf power is essential, e.g. to eliminate bulky rf pre-amplifiers or in medical high-field MRI to preserve patient safety. Another benefit of the new scheme are very short dead times allowing for measurements of samples with short relaxation times. In this work, Frank-sequence excitation is used for low-power imaging for the first time. Results of one-, two-, and three-dimensional imaging experiments are presented and compared to conventional images.

1. Introduction

Since the beginning of Magnetic Resonance Imaging (MRI) approximately 40 years ago, the strength of the main magnetic field has steadily increased by several orders of magnitude, from a few millitesla in permanent magnets to over 9 T in modern super-conducting tomographs. Along with it, advances have been made regarding homogeneity and temporal stability of the fields. While 1.5–3 T tomographs are clinical standard since the 1990s, the use of ultra high fields of 7 T up to 11 T is restricted mainly to research applications. On the one hand, high field strengths offer the great advantage of an intrinsically higher sensitivity leading to a higher Signal-to-Noise Ratio (SNR) and thus higher spatial and temporal resolution. This allows for many new applications of MRI, in particular imaging of brain function. On the other hand, new issues arise: acoustic noise of more than 100 dB(A) generated by mechanical deformation of the gradient coils during switching is an important drawback of ultra high-field MRI [1]. Moreover, due to increased susceptibility effects and changes in spin relaxation times, T_1 and T_2, image quality may be lost [2,3]. It therefore is essential to provide pulse sequences that also allow for measurements of short relaxation times. Another critical aspect is the permanently exceeded Specific Absorption Rate (SAR) limit defined as the energy absorbed by body tissue per unit time and body weight [4]. Since it scales with the square of the main magnetic field strength, only small improvements have been achieved by modified radio-frequency (rf) coils and pulse sequences [5–7]. Consequently, rf energy needs to be reduced, which can be realized by decreasing peak rf power and total measurement time.

A recently introduced new pulse excitation scheme, *Frank-sequence excitation* [8], employs rf pulses with peak rf powers that are reduced by a factor of the order of 10^3 and higher compared to conventional hard pulse excitation. A similar new sequence called SWeep Imaging with Fourier Transformation (SWIFT) has been shown to yield power reduction levels of typically two orders of magnitude [9,10]. Even though total rf energy cannot be saved by Frank excitation, it is distributed over the entire scan time thereby decreasing unfavorable effects. Additionally, the sequence does not require any recycle delay. Its time-shared mode of excitation and acquisition is well-suited for measurement of short relaxation times. The application of this pulse scheme on MRI is shown for the first time and is compared to standard imaging. In order to achieve slice selection while maintaining low-power excitation, Frank excitation is combined with a technique called Selective Pulses with Reduced Amplitude Distribution (SPREAD) [11] yielding three-dimensional MRI results.

2. Theory

2.1. The Frank sequence

Frank-sequence excitation NMR has been introduced in [8] and a detailed derivation can be found therein. Thus, only a brief summary is given here. As one special type of Frank sequences, which have commonly been used in communication theory [12–14], so-called *polyphase perfect sequences* are employed. Their main feature is the constant absolute value of both the function itself and its Fourier transform. This leads to white excitation, where white refers to the discrete frequency axis that results from discrete Fourier transformation of the Frank function defined on a discrete

* Corresponding author. Fax: +49 241 8022185.
E-mail address: amor@itmc.rwth-aachen.de (N. Amor).

1090-7807/$ - see front matter © 2011 Elsevier Inc. All rights reserved.
doi:10.1016/j.jmr.2011.05.004

time grid. If the Fourier transformation is executed on a continuous time axis, then the excitation function is a sinc-shape defined by the Fourier transformation of one excitation pulse. Frank sequence exciation yields minimal peak rf power, since for constant rf amplitudes, the average power can be considered equal to the peak power.

Since the absolute value is to remain constant, only the phase is modulated. For Frank excitation, the rf carrier phase is modulated by rotating waves:

$$x(t) = \exp(i2\pi ft), \tag{1}$$

with m discretized frequencies,

$$f = \frac{f_w}{m\Delta t}, \quad m \in \mathbb{N}, \quad 0 \leqslant f_w < m, \quad \Delta t = DW. \tag{2}$$

On a discrete time grid, as in experiments with digital signal sampling,

$$t = t_w \Delta t, \quad 0 \leqslant t_w < m \tag{3}$$

the final expression for the Frank sequence is:

$$x(t_n \Delta t) = \exp\left(i2\pi \frac{f_w t_w}{m}\right). \tag{4}$$

The parameters t_w and f_w are equivalent to counters for steps in time and frequency, respectively, within each one of m wave packages. One Frank scan contains m wave packages and a total of $N = m^2$ pulses, applied in time intervals of $\Delta t = DW$ (dwell time) with the phases specified by Eq. (4). Data acquisition is performed in a time-shared way by interleaving acquisition of one complex data point per DW. Raw data then needs to be Fourier-transformed and deconvolved. Since acquisition occurs directly after each pulse, samples with very short relaxation times can be measured by Frank NMR, like in Single-Point Imaging (SPI) [15]. In some cases, this condition has lately been described as allowing for zero echo time, $TE = 0$ [9,10,16]. However, since no echo is formed, an echo time does not really exist and therefore, this term will not be used in the following.

The special phase modulation basically translates into an excitation of a fraction of $1/m$ of the entire excitation bandwidth for each Frank wave package. With each package, a different band is excited. Thus, a full Frank scan discretely sweeps through the frequency range defined by $1/\Delta t$.

The savings in peak rf power gained by extending the excitation from a single pulse to a string of m^2 constant-amplitude pulses can be approximated in the linear limit by comparing the power spectral densities, which are the Fourier transforms of the auto-correlations $R_{x,x}(\tau)$ of the excitation functions $x(t)$. Assuming each pulse to last one time step Δt, one obtains for the conventional 90° pulse:

$$x_{90}(t) = B_{1,90}[\Theta(t) - \Theta(t - \Delta t)], \tag{5}$$

where $B_{1,90}$ is the amplitude of the rf radiation and $\Theta(t)$ is the Heaviside step function. This leads to

$$R_{x_{90},x_{90}}(\tau)|_{\tau=0} := \int_{-\infty}^{\infty} x_{90}(t)x_{90}(t-\tau)dt|_{\tau=0} = B_{1,90}^2 \Delta t. \tag{6}$$

The equivalent calculation for the Frank excitation gives:

$$R_{x_{Frank},x_{Frank}}(\tau)|_{\tau=0} = B_{1,Frank}^2 T. \tag{7}$$

With $T = m^2\Delta t$, the comparison yields the result that for equal power spectral densities, it is required that

$$B_{1,90} = mB_{1,Frank}. \tag{8}$$

If one also takes into consideration, that the rf pulse of length Δt_p has to be shorter or equal to half the dwell time [8], Eq. (8) becomes:

$$B_{1,90} = m\frac{\Delta t_p}{\Delta t} B_{1,Frank} \leqslant \frac{m}{2} B_{1,Frank}. \tag{9}$$

Consequently, total rf energy cannot be saved by the Frank sequence. This deviation corrects an error in the original publication [8], where a power savings of a fraction of m^4 was claimed, instead of m^2.

2.2. Filtered backprojection imaging

For conventional MRI, the dephasing of transverse magnetization is typically refocused by either a 180° pulse in a spin echo (SE) sequence or by making use of a gradient echo (GE). Besides an increase in sensitivity, echo imaging allows for frequency and phase encoding within one scan leading to linear k-space sampling. The Cartesian data set can then easily be processed with Fast Fourier Transformation (FFT) algorithms.

Since linear Frank-sequence excitation does not give rise to echoes, only frequency encoding can be applied. Therefore, k-space needs to be sampled in other ways, e.g. radially or spirally. In this work, Filtered Backprojection (FBP) [17–19] was employed, i.e. one-dimensional profiles are acquired along various spatial directions and the real image is reconstructed by filtering and Radon-transforming the data set. A scheme of the Frank FBP pulse sequence is demonstrated in Fig. 1.

Even though the acquisition of non-Cartesian k-space sampling and the necessary interpolation to a Cartesian grid for FFT requires more advanced post-processing and sometimes leads to image artifacts, it offers a great advantage over echo imaging schemes: because the gradients are only stepped in very small increments to yield small changes in acquisition angles, radial imaging reduces acoustic noise to a minimum. Thus, any radial imaging scheme circumvents high noise levels.

2.3. SPREAD slice selection

In order to maintain the advantage of low-power excitation also in slice selection, which is essential for physiological MRI, an alternative to standard excitation needs to be employed. Conventionally, a clipped, sinc-shaped rf pulse ($\sin c(x) = \sin(x)/x$) is applied under a magnetic field gradient and transforms the longitudinal magnetization within a well-defined frequency band into detectable transverse magnetization (Fig. 2). Alternatively, the fractions of longitudinal magnetization associated with frequencies outside the relevant slice can be pre-saturated before any non-selective excitation scheme is employed, e.g. Frank sequences, to make use of the remaining magnetization. This approach was first realized by the so-called DIGGER pulses (Discrete Isolation from Gradient Governed Elimination of Resonances) [20], for which an inverse Fourier transformation of the inverted frequency excitation profile leads to a narrow distribution of the amplitudes in the time domain. Another advantage of pre-saturating unnecessary magnetization is the fact that the saturating rf irradiation does not need to be phase coherent. The hereby gained degree of freedom can be used for a reduction of peak rf power: the SPREAD method (Selective Pulses with Reduced Amplitude Distribution) is explained in detail in [11]. In Fig. 3, the idea of the construction and implementation of SPREAD pulses is reviewed: After choosing the slice width $\Delta\omega$, the remaining frequencies within the total band under investigation, $\Delta\Omega$, are assigned a random phase. Inverse Fourier Transformation (IFT) then yields the phase and amplitude of the rf pulse. When applied in a preparation block that includes a slice selection gradient, any experiment can be performed afterwards, which will only detect magnetization from within the relevant slice. In the example given, the excitation is a single non-selective pulse for observation of an FID. Since usually

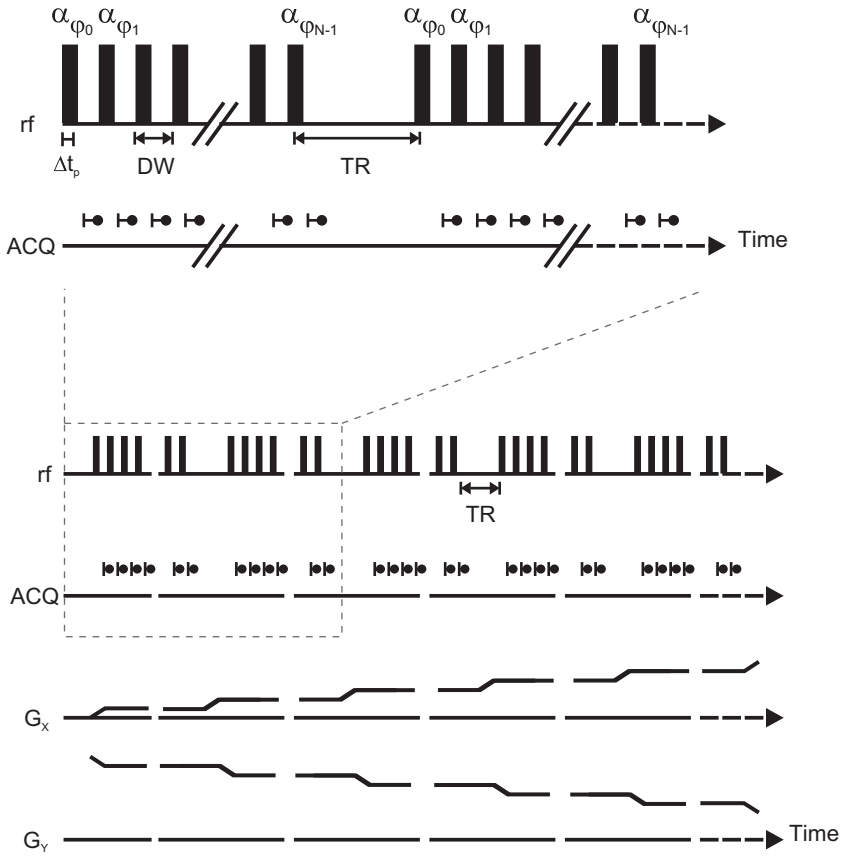

Fig. 1. Schematic drawing of a Frank excitation pulse sequence (top) integrated into radial imaging (bottom). The acquisition is interleaved with the *N* rf pulses. During each of the scans, a gradient is applied to encode the profiles needed for FBP.

one of these SPREAD pulses does not completely saturate unnecessary magnetization, several different pulses are applied in between successive scans. In order to avoid unwanted echo formation, these pulses should differ from each other in their phase and amplitude modulations.

3. Materials and methods

Experiments were performed on a Bruker DSX 200 MHz spectrometer equipped with a Micro 2.5 gradient system with a maximum strength of 1 T/m and using standard 10 mm and 20 mm Bruker birdcage resonators. The Frank sequence was realized with $m = 32$, yielding a total number of pulses of $N = 1024$ and thus an according number of acquired complex data points. The Frank-sequence frequency sweep was started with the central frequencies. For backprojection imaging, profiles were acquired in steps of 1° to cover the entire *k*-space with sufficiently high resolution. Raw data was subjected to FFT and deconvolution and was filtered and Radon-transformed employing linear interpolation. The filter chosen for the images presented here was the so-called Hamming-filter, which is standard for FBP and is constructed from a ramp filter multiplied by a Hamming window to reduce noise sensitivity.

Because image quality can more reliably be evaluated for known samples, two different phantoms were asse mbled: the first (Fig. 4a) consisted of four small glass tubes of 3 mm inner diameter (ID), which were filled to different levels with $CuSO_4$-doped water with a spin–lattice relaxation time of $T_1 = 850$ ms to introduce image contrast. The second one was more complex (Fig. 4b). Two nested glass cylinders produced a ring-shaped gap of approximately 2 mm which was completely filled with $CuSO_4$-doped water ($T_1 = 500$ ms). Inside the inner cylinder 20 glass capillaries with OD of 1 mm were placed, which again were filled to different levels with the same doped water.

4. Results and discussions

4.1. 2D MRI

A comparison of standard and Frank-sequence MRI was first made on 2D images of the simpler glass tube phantom (Fig. 5).

Despite the reduction of rf power from 32 W to only 0.1 W and the enormous time savings, the Frank image exhibits equally high quality as the conventional SE image: in both images the regions of the water-filled tubes are well-distinguishable from the background and the contrast introduced by the varying filling degrees is clearly observable. Since the tubes could not be aligned perfectly, the projection images do not show exact circles, particularly for the upper and the bottom tube. In the standard image (a), these regions appear to be blurred, while the backprojection image (b) represents slightly deformed edges. This effect has been found to be even more pronounced in a FBP image using standard excitation (cf. Supporting Material, Fig. A.9). Owing to the frequency sweep character of the Frank-sequence excitation, the recycle delay could be reduced from 2.5 s in the SE image to a minimum of only 100 ms for the Frank sequence. The short delay was set due to soft- and hardware requirements even though it leads to some loss in signal.

The same experiment was performed using the more complex phantom (Fig. 6). The Frank image principally reproduces intensities and shapes of the phantom very well. Contrast introduced by varying water levels is depicted correctly. The artifacts in the corners are due to the Hamming filter used in the backprojection

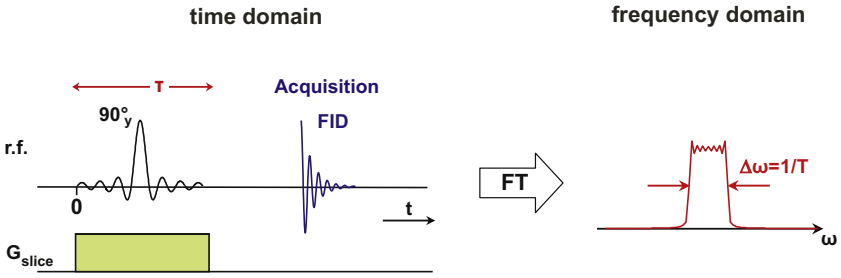

Fig. 2. Illustration of a simple pulse program for slice selection by direct generation of transverse magnetization with a sinc-shaped rf pulse, which is applied simultaneously with a slice selection gradient pulse. Fourier transformation yields the desired profile, which experiences distortions due to the truncation of the sinc-pulse.

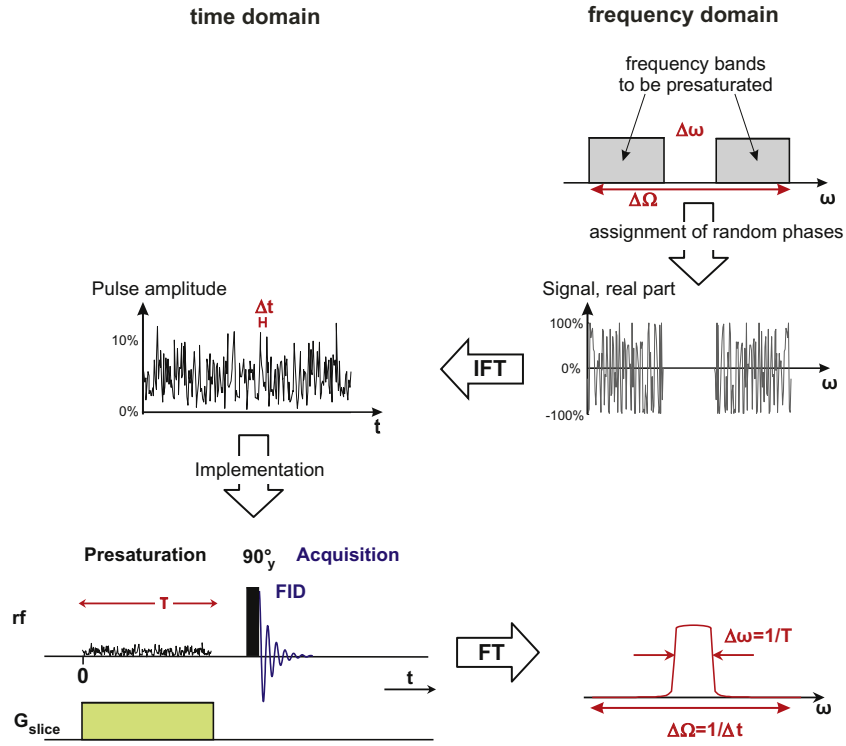

Fig. 3. Illustration of the construction of a SPREAD pulse and its implementation into a simple pulse program for slice selection by pre-saturation of longitudinal magnetization between successive scans. The SPREAD pulse is designed according to the desired profile shape and applied together with the selection gradient pulse. The signal is read out after a standard rf pulse and processed by Fourier transformation.

procedure. In the center, noise leads to a ring-shaped artifact. The same effect has been observed in a FBP acquired with standard hard pulse excitation (c.f. Supporting Material, Fig. A.10 and thereby has been proven to be independent of the Frank method itself. A constant colored noise peak outside the sample has been filtered during post-processing in order to avoid distortions introduced in the FBP. The ruffled edge of the outer ring is caused by partially non-white excitation, as the rf power of only 0.1 W still exceeded the limit for true linearity which is asked for in the Frank sequence design. It was chosen that high to increase the effective flip angle and consequently, circumvent sensitivity losses. Thus, each of the $m = 32$ Frank packages becomes discriminable in the image. A more detailed analysis of this effect will be discussed in a separate publication. The repetition time was decreased again, so the total experiment time was reduced from 13.13 min to only 2.65 min. For equal SNR, numbers of averages, matrix sizes and FOV, a time saving of almost a factor of four was calculated.

4.2. Slice selection

To measure 2D slice-selective images instead of 2D projections, the low-power SPREAD method was implemented and tested on a standard 10 mm NMR tube with an ID of 8 mm filled with $CuSO_4$-doped water. Fig. 7 shows the direct comparison of sinc-excitation and the SPREAD technique by 1D images. The gray line marks the conventionally acquired complete 1D profile along the *Z*-axis, out of which slices of 6.25 mm were to be excited by sinc-shaped and SPREAD pulses. Side bands are excited by the finite and thus only approximately sinc-shaped pulse (Fig. 7a). The SPREAD pulse produced very sharp slice edges and very good signal saturation in the surrounding (Fig. 7b). However, unwanted echo formation by the series of SPREAD pulses has led to an excitation pattern within the slice, which has remained despite the application of varying pulse shapes. The use of SPREAD pulses allowed a reduction of rf power from 32 W to 0.3 W.

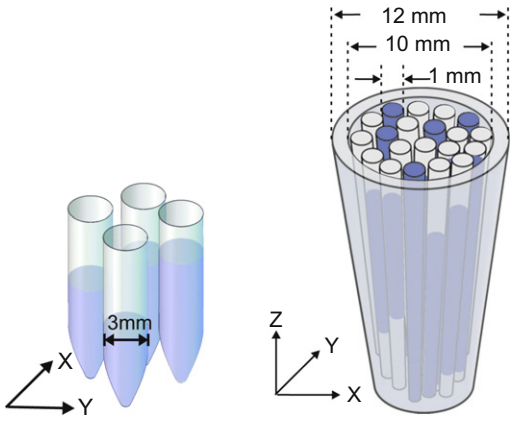

(a) Glass tube phantom (b) Capillary phantom

Fig. 4. (a) Imaging phantom consisting of four glass tubes of 3 mm ID, which were filled to different levels with $CuSO_4$-doped water. (b) Sketch of the capillary phantom, which consists of two nested glass cylinders with a fluid-filled gap of approx. 2 mm and 20 glass capillaries that were filled to different levels. The sample was again partially filled with $CuSO_4$-doped water.

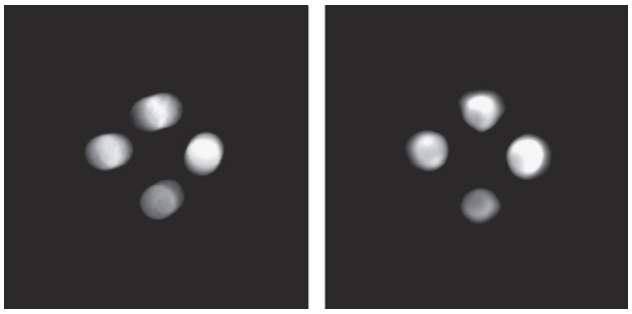

(a) Conventional excitation, SE (b) Frank sequence, FBP

Fig. 5. Two-dimensional projection images of the phantom depicted in Fig. 4a onto the transverse (*XY*) plane. FOV = (32 × 32) mm^2. (a) Original matrix size = (256 × 256) Px^2, twofold zero-filling, echo time TE = 5 ms, signal averaged over NS = 8 scans, repetition time TR = 2.5 s, total scan time = 85.47 min, SNR = 1155. 256 rf pulses per scan of 25.9 μs at 32 W, flip angle = 90°. (b) Profiles in increments of 1°, FBP by linear interpolation and Hamming filtering, matrix size = (1024 × 1024) Px^2; NS = 1, TR = 100 ms, total scan time = 0.82 min, SNR = 337. 361 × 1024 rf pulses of 10.0 μs at only 0.1 W, flip angle = 2°.

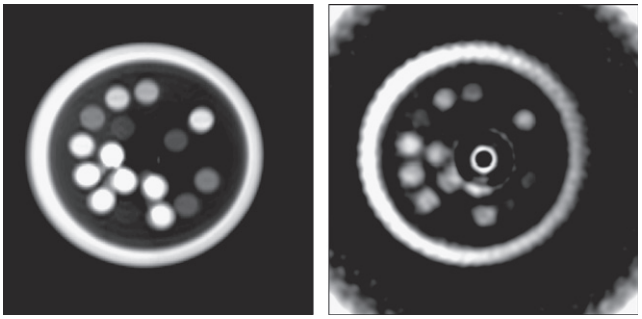

(a) Conventional excitation, SE (b) Frank sequence, FBP

Fig. 6. Two-dimensional MR projection images of the capillary phantom shown in Fig. 4b onto the transverse (XY) plane. (a) FOV = (15 × 15)mm^2, original matrix size = (128 × 64) Px^2, 4-fold zero-filling, TE = 10 ms, NS = 16, TR = 3 s, total scan time = 13.13 min, SNR = 904. 128 rf pulses per scan of 36 μs were employed at 32 W, flip angle = 90°. (b) Original FOV = (21 × 21) mm^2, original matrix size = (1024 × 1024) Px^2, NS = 4, TR = 50 ms, total scan time = 2.65 min, SNR = 6. 361 rf pulses per scan of 10 μs at only 0.1 W, flip angle = 2°.

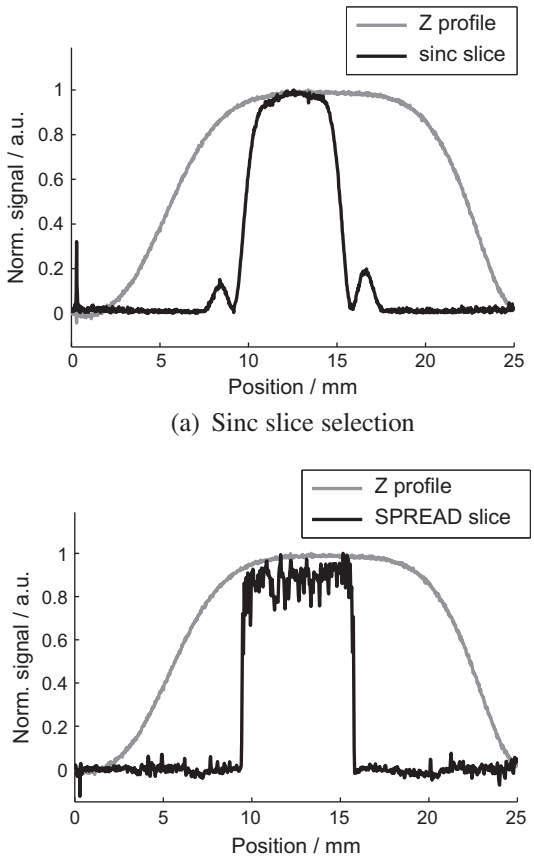

(a) Sinc slice selection

(b) SPREAD slice selection

Fig. 7. Comparison of conventional and SPREAD slice selection by comparing slices through one-dimensional profiles of the NMR tube (ID = 8 mm) along the *Z* axis. FOV = 25 mm, matrix size = 1024 Px, slice thickness = 6.25 mm. (a) Sinc slice. One rf pulse for slice selection of 2000 μs at 32 W, flip angle = 90°. (b) SPREAD presaturation followed by conventional hard pulse. 20 SPREAD rf pulses of 2560 μs at only 0.3 W, followed by one rf pulse of 36 μs at 32 W, flip angle = 90°.

4.3. Slice-selective 2D MRI

Finally, both low-power NMR techniques, Frank excitation and SPREAD, examined separately in Sections 4.1 and 4.2 were combined to yield slice-selective two-dimensional images of the capillary phantom. Fig. 8 illustrates again the comparison of

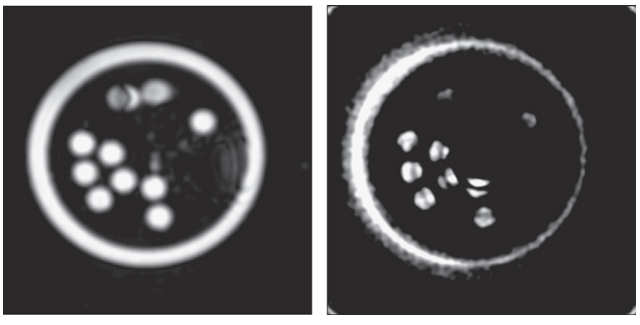

(a) Conventional (b) Low-power methods

Fig. 8. Slice-selective two-dimensional MR images of the capillary phantom shown in Fig. 4b onto the transverse (*XY*) plane. Slice thickness = 5 mm. (a) FOV = (15 × 15) mm^2, original matrix size = (64 × 64) Px^2, 4-fold zero-filling, NS = 4, TR = 3 s, total scan time = 13.03 min, SNR = 337. 64 rf excitation (90°) pulses per scan of 36 μs at 32 W and 64 refocusing pulses (180°) of 500 μs at 16 W. (b) Original FOV = (21 × 21) mm^2, matrix size = (1024 × 1024) Px^2, NS = 4, TR = 50 ms, total scan time = 5.12 min, SNR = 13. 361 × 20 SPREAD pulses per scan of 2560 μs at 0.3 W and 361 × 1024 Frank pulses (0.13°) of 10 μs at 0.16 W.

conventional MRI, i.e. a sinc pulse SE image, and the new methods. The slice selection reduced the SNR, so the difficulties with SPREAD, Frank excitation, and FBP discussed above add up and become more prominent. Nevertheless, the most important features of the sample are reproduced. The outer ring shows a variation of the thickness which is caused by a dislocation of the inner glass tube from the center of the outer tube. As for previous images, rf power was reduced by several orders of magnitude and total scan time with the new low-power methods was less than half of the time needed for the conventionally acquired image.

A direct, quantitative comparison of all SNR values is difficult because identical acquisition conditions and spectrometer filters have to be assured. Also, the comparison requires the backprojection from cylindrical to cartesian coordinates to employ identical filters. When using the SNR normalized to the pixel area A of the final image and to the square root of the total acquisition time $\sqrt{t_{acq}}$, then for the slice selective images of Fig. 8, comparable values are obtained ($SNR^{SE}/\left(A^{SE}\sqrt{t_{acq}^{SE}}\right) = 2.7 \times 10^4\ \mathrm{Px}^2/(\mathrm{mm}^2\sqrt{\mathrm{min}})$; $SNR^{FBP}/\left(A^{FBP}\sqrt{t_{acq}^{FBP}}\right) = 1.4 \times 10^4\ \mathrm{Px}^2/(\mathrm{mm}^2\sqrt{\mathrm{min}})$). A thorough comparison will be subject of another publication.

5. Conclusions and outlook

In the work presented, it could be shown for the first time that Frank-sequence excitation allows for reduction of rf peak power in MRI by several orders of magnitude and of total acquisition time while still maintaining image quality. Two-dimensional MRI has been successfully performed and extended to slice-selective imaging routines employing a combination of the SPREAD and Frank schemes.

In conclusion, Frank MRI greatly profits from the extension of total rf power over the acquisition time because peak rf power decreases in proportion to the number of time increments, which is equal to the number of rf pulses. Generally, the upper limit of this number is only given by NMR spectrometer performance. However, the full potential of Frank MRI with regard to time savings is somewhat compromised by sensitivity losses when performing the Frank sequence in the linear excitation regime, which is necessary to prevent artifacts from non-linear excitation. When averaging over more scans, the acquisition time increases quadratically with the gain in SNR. The radial imaging scheme used for FBP allows for smooth gradient switching and thereby effectively reduces acoustic noise.

In future applications, artifacts arising from the filtered backprojection algorithm can be avoided by referring to the more advanced method of *gridding* instead [21]. For three-dimensional MRI, an encoding gradient can be used in addition to the 2D imaging scheme presented here. Because only Frank excitation is used then, maximal power reduction can be achieved. Also for slice selection, further reduction of rf peak power and even of total rf energy can be achieved by application of separate wave packages of the Frank sequences instead of the SPREAD pre-saturation block. The Frank wave package, applied under a slice selection gradient, will only excite a defined section of the complete spectral bandwidth.

Appendix A. Supplementary data

Supplementary data associated with this article can be found, in the online version, at doi:10.1016/j.jmr.2011.05.004.

References

[1] T.F. Budinger, H. Fischer, D. Hentshel, H.E. Reinfelder, F. Schmitt, Physiological effects of fast oscillating magnetic field gradients, J. Comput. Assist. Tomogr. 15 (1991) 609–614.
[2] P. Jezzard, S. Duewell, R.S. Balaban, MR relaxation times in human brain: measurement at 4 T, Radiology 199 (1996) 773–779.
[3] J.P. Wansapura, S.K. Holland, R.S. Dunn, W.S. Ball, NMR relaxation times in the human brain at 3.0 Tesla, J. Magn. Reson. Imag. 9 (1999) 531–538.
[4] IEC 60601-2-33: Medical Electrical Equipment – Particular Requirements for the Safety of Magnetic Resonance Equipment for Medical Diagnosis, July 2008.
[5] J.T. Vaughan, M. Garwood, C.M. Collins, W. Liu, L. DelaBarre, G. Adriany, P. Andersen, H. Merkle, R. Goebel, M.B. Smith, K. Ugurbil, 7 T vs. 4 T: RF power, homogeneity, and signal-to-noise comparison in head images, Magn. Reson. Med. 46 (2001) 24–30.
[6] P.A. Bottomley, E.R. Andrew, RF magnetic-field penetration, phase-shift and power dissipation in biological tissue implications for NMR imaging, Phys. Med. Biol. 23 (1978) 630–643.
[7] P.M. Robitaille, A.M. Abduljalil, A. Kangarlu, X. Zhang, Y. Yu, R. Burgess, S. Bair, P. Noa, L. Yang, H. Zhu, B. Palmer, Z. Jiang, D.M. Chakeres, D. Spigos, Human magnetic resonance imaging at 8T, NMR Biomed. 11 (1998) 263–265.
[8] B. Blümich, Q. Gong, E. Byrne, M. Greferath, NMR with excitation modulated by Frank sequences, J. Magn. Reson. 199 (2009) 18–24.
[9] D. Idiyatullin, C. Corum, J.-Y. Park, M. Garwood, Fast and quiet MRI using a swept radiofrequency, J. Magn. Reson. 181 (2006) 342–349.
[10] D. Idiyatullin, C. Corum, S. Moeller, M. Garwood, Gapped pulses for frequency-swept MRI, J. Magn. Reson. 193 (2008) 267–273.
[11] H. Nilgens, M. Thelen, J. Paff, P. Blümler, B. Blümich, Hadamard NMR imaging with slice selection, Magn. Reson. Imag. 14 (1996) 857–861.
[12] R. Heimiller, Phase shift pulse codes with good periodic correlation properties, IRE Trans. Inf. Theory IT-7 (1961) 254–257.
[13] R. Heimiller, Authors comment, IRE Trans. Inf. Theory IT-8 (1962) 382.
[14] P. Fan, M. Darnell, Sequence Design for Communications Applications, John Wiley & Sons Inc., New York, 2000.
[15] S. Emid, J.H.N. Creyghton, High resolution NMR imaging in solids, Physica B+C 128 (1) (1985) 81–83.
[16] M. Robson, M. Gatehouse, M. Bydder, G. Bydder, Magnetic resonance: an introduction to ultrashort TE (UTE) imaging, J. Comput. Assist. Tomogr. 27 (2003) 824–846.
[17] J. Radon, Über die Bestimmung von Funktionen durch ihre Integralwerte längs gewisser Mannigfaltigkeiten, Berichte Sächsischer Akademie der Wissenschaften zu Leipzig, Math. Phys. Klasse 69 (1917) 262–267.
[18] A. Kak, M. Slaney, Principles of Computerized Tomographic Imaging, IEEE Press, New York, NY, 1988.
[19] R.N. Bracewell, Two-Dimensional Imaging, Prentice Hall, Englewood Cliffs, NJ, 1995.
[20] D.M. Doddrell, J.M. Bulsing, G.J. Galloway, W.M. Brooks, J. Field, M. Irving, H. Baddeley, Discrete isolation from gradient-governed elimination of resonances. DIGGER, a new technique for in vivo volume-selected NMR spectroscopy, J. Magn. Reson. 70 (1986) 319–326.
[21] J. Jackson, C. Meyer, D. Nishimura, A. Macovski, Selection of a convolution function for Fourier inversion using gridding, IEEE Trans. Med. Imag. 10 (1991) 473–478.